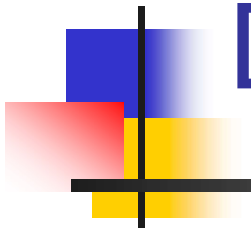

Deformação Plástica

A fonte de Frank-Read

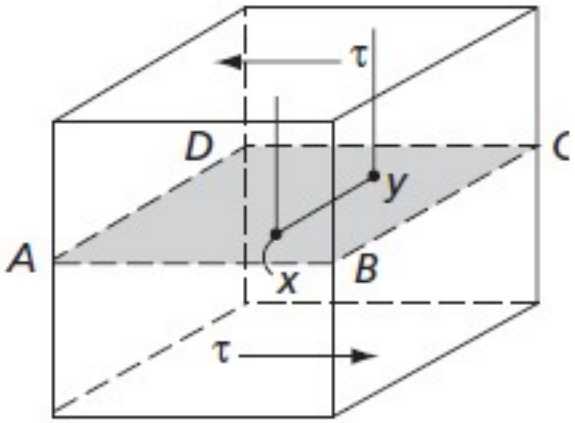

FIG. 5.1 Frank-Read source. The dislocation segment *xy* may move in plane *ABCD* under the applied stress. Its ends, *x* and *y*, however, are fixed

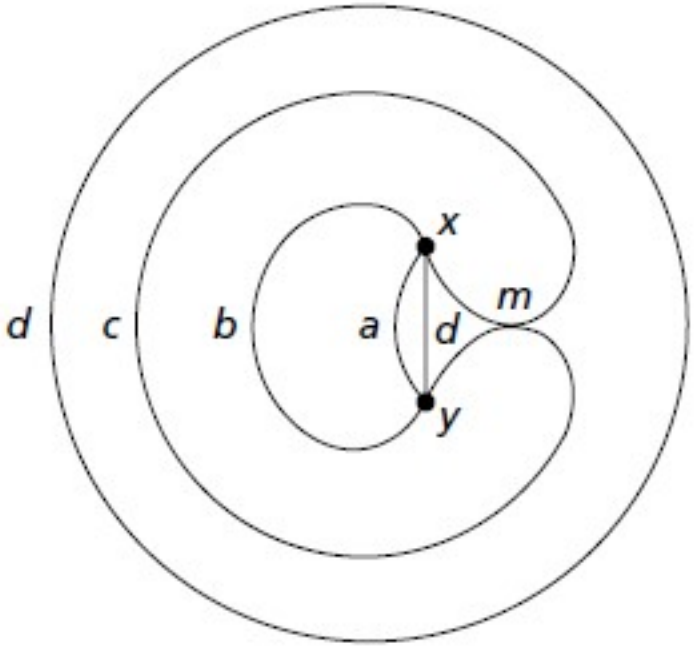

FIG. 5.2 Various stages in the generation of a dislocation loop at a Frank-Read source

Filme

A fonte de Frank-Read

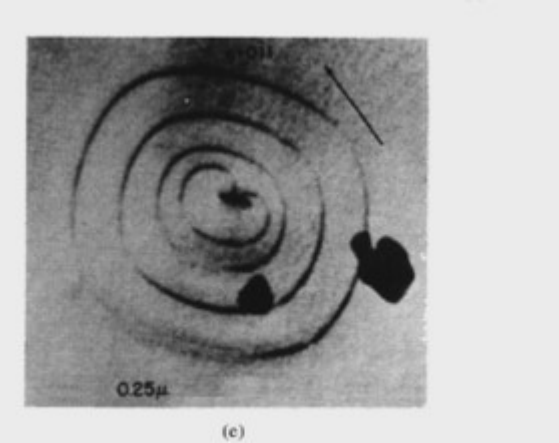

J. Brittain, Met. Trans. 6A, 1975

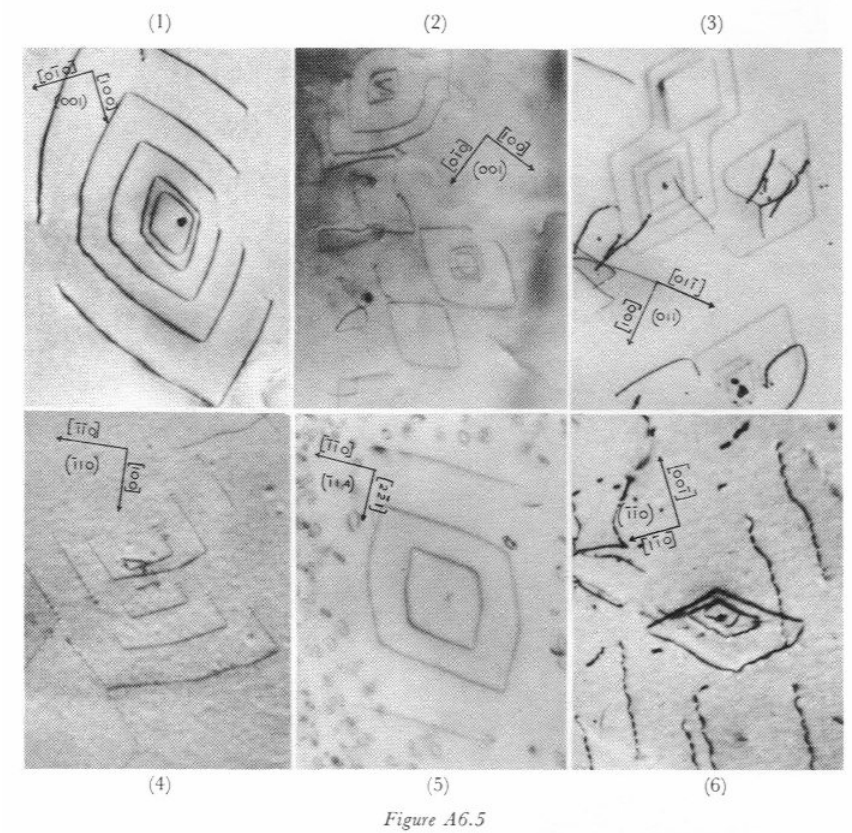

Figure A6.5

University of Rice

Nucleação de discordâncias

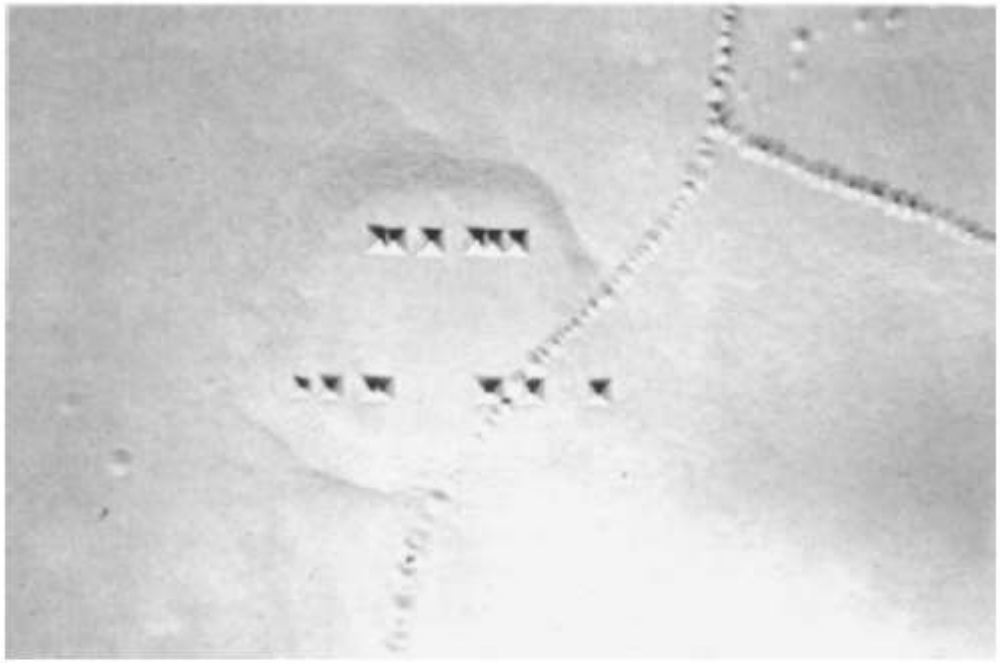

FIG. 5.3 The large square etched pits in horizontal rows correspond to dislocations formed in LiF at room temperature, while the smaller, closely spaced pits lying in curved rows were grown into the crystal when it was manufactured (Gilman, J. J., and Johnson, W. G., *Dislocations and Mechanical Properties of Crystals*, p. 116, John Wiley and Sons, Inc., New York, 1957. Used by permission of the author.)

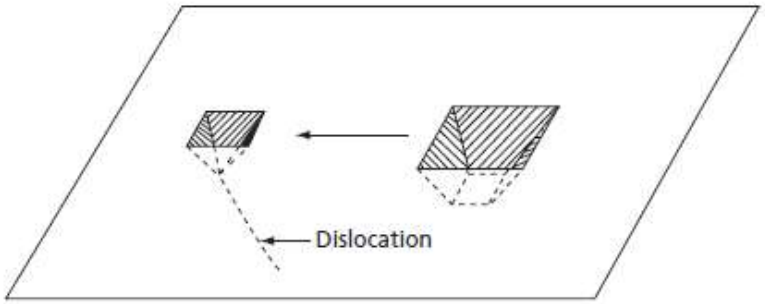

FIG. 5.4 Dislocation movement in LiF as revealed by repeated etching (Reprinted with permission from J.J. Gilman and W.G. Johnson, *Journal of Applied Physics*, Vol. 30, Issue 2, Page 129, Copyright 1959, American Institute of Physics)

Deformação plástica em flexão

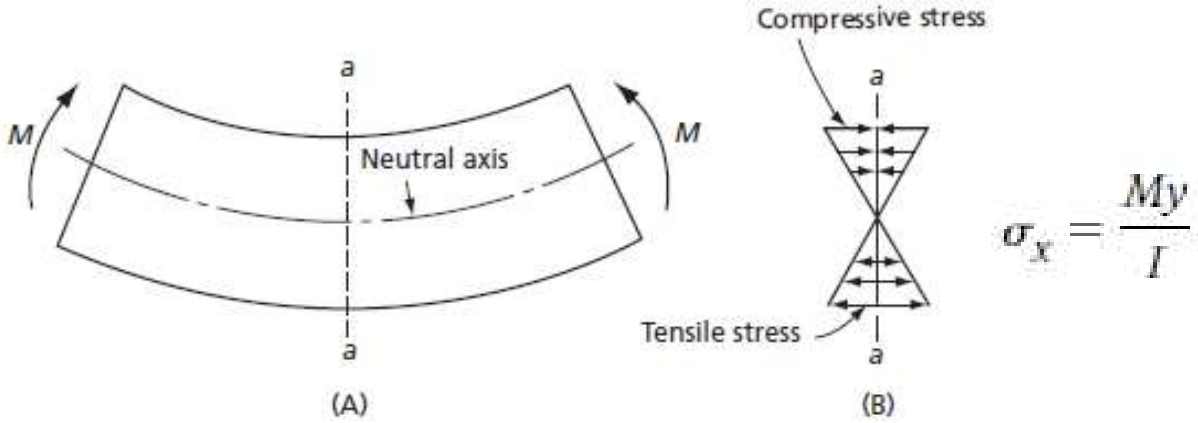

$$\sigma_x = \frac{My}{I}$$

FIG. 5.5 (A) The elastic deformation of a crystal subject to two equal moments (M) applied at its ends. **(B)** The normal stress distribution on a cross-section such as aa

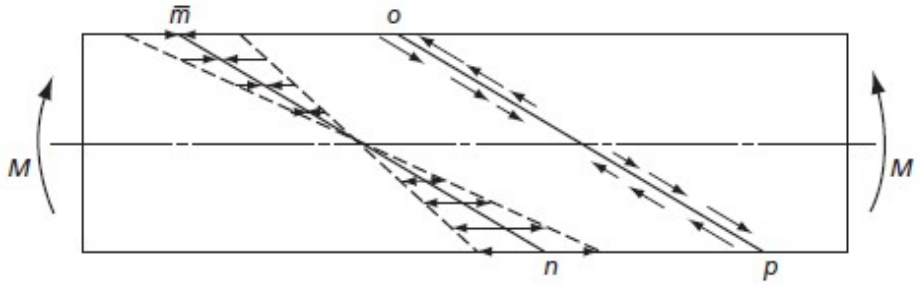

FIG. 5.6 The stress distribution on slip planes corresponding to the elastic deformation shown in Fig. 5.5

Deformação plástica em flexão

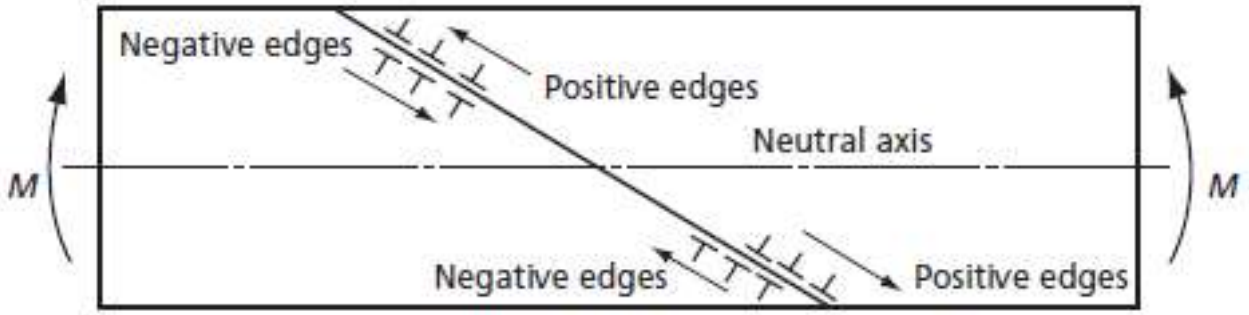

FIG. 5.7 The effect of the stress distribution on the movement of dislocations. Positive-edge components move toward the surface; negative edges toward the neutral axis

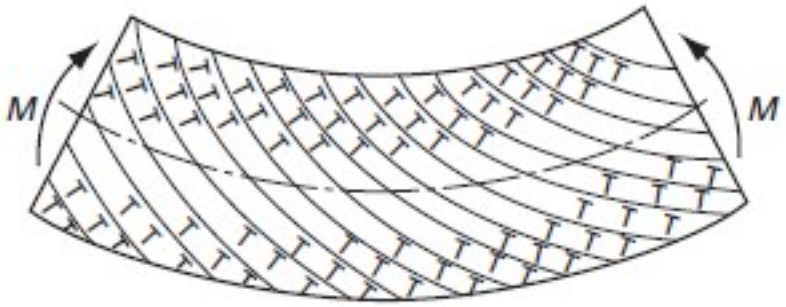

FIG. 5.8 Distribution of the excess edge dislocations in a plastically bent crystal

Deformação plástica em torsão

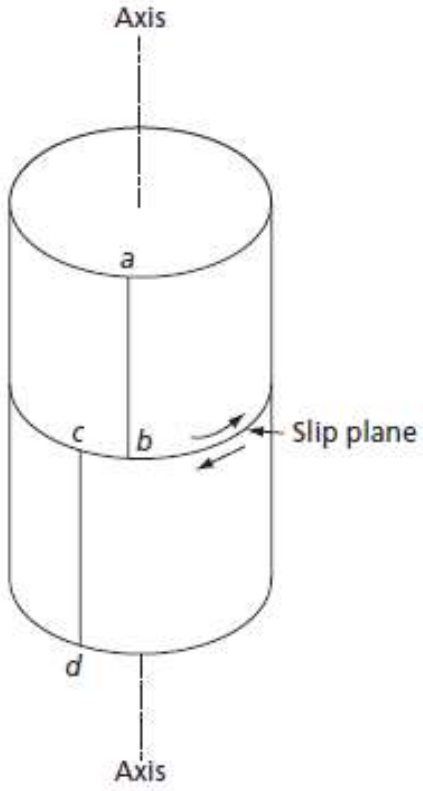

FIG. 5.9 A single crystal can be rotated about an axis normal to a slip plane that contains several slip directions

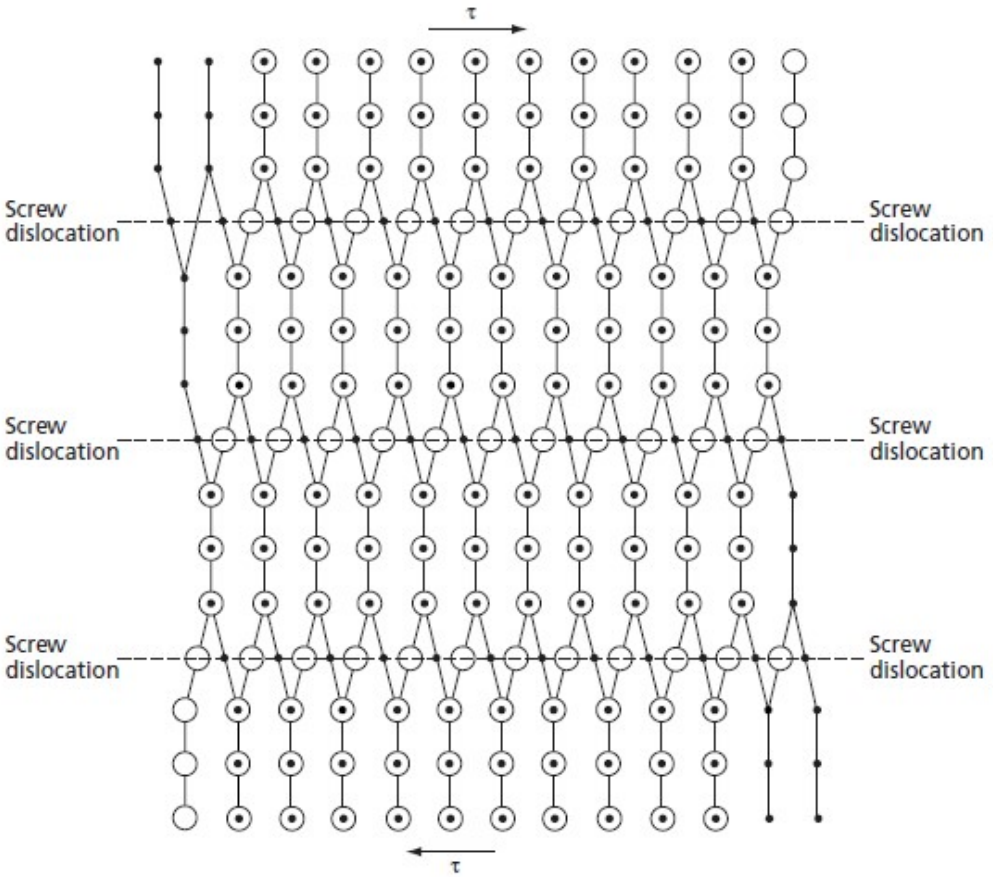

FIG. 5.10 An array of parallel screw dislocations. Open circles represent atoms just above the slip plane, while dots correspond to atoms just below it

Deformação plástica em torsão

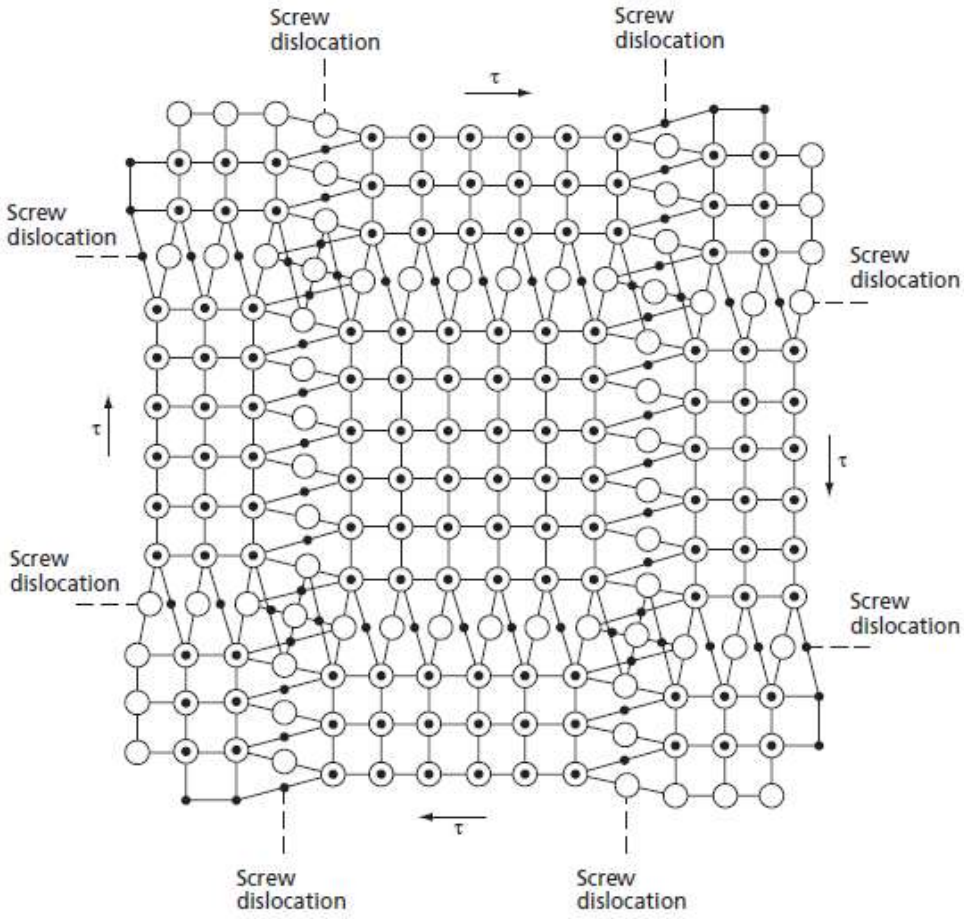

FIG. 5.11 A double array of screw dislocations. This array does not have a long-range strain field; open circles show atoms above the slip plane, while dots represent those below the plane

Planos e direções de cisalhamento

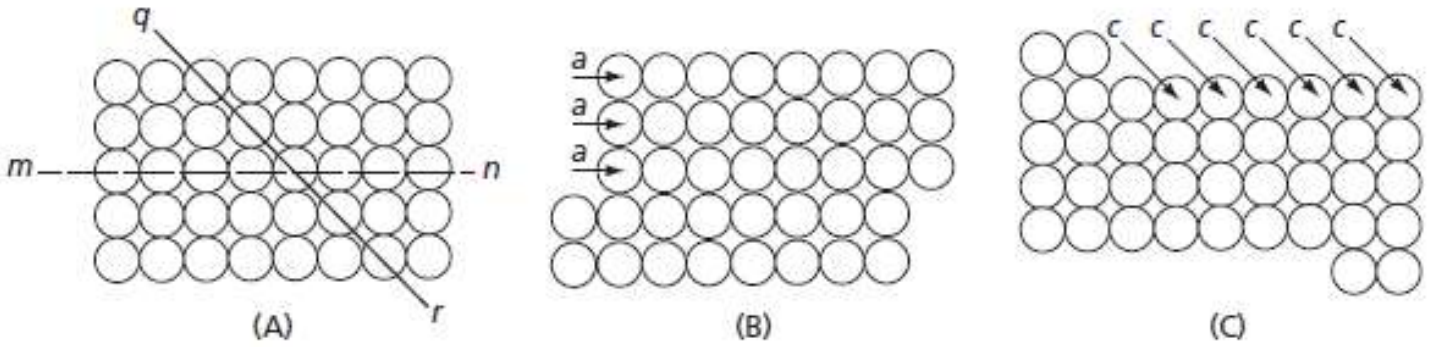

FIG. 5.12 Two ways in which a simple cubic lattice can be sheared while still maintaining the lattice symmetry: **(A)** Crystal before shearing, **(B)** shear in a close-packed direction, and **(C)** shear in a non-close-packed direction

A combinação de um plano compacto com uma de suas respectivas direções compactas definem um "sistema (ou modo) de escorregamento".

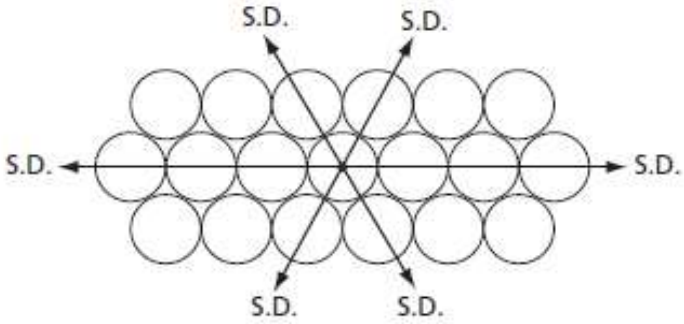

FIG. 5.13 The three slip directions (S.D.) in a plane of closest packing. Notice that this type of plane occurs in both the hexagonal close-packed and the face-centered cubic lattices

Tensão crítica de cisalhamento

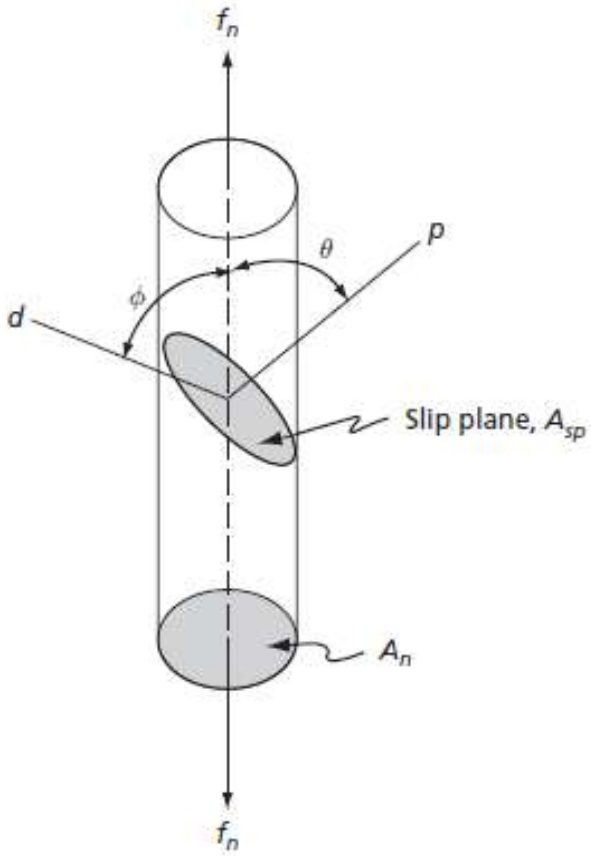

FIG. 5.14 A figure for the determination of the critical resolved shear stress equation

$$A_{sp} = \frac{A_n}{\cos\theta} \qquad \sigma_A = \frac{f_n}{A_{sp}} = \frac{f_n}{A_n}\cos\theta$$

$$\tau = \sigma_A \cos\phi = \frac{f_n}{A_n}\cos\theta\cos\phi$$

$$\tau = \sigma \cos\theta \cos\phi$$

Equação de Schmid

Tensão crítica de cisalhamento

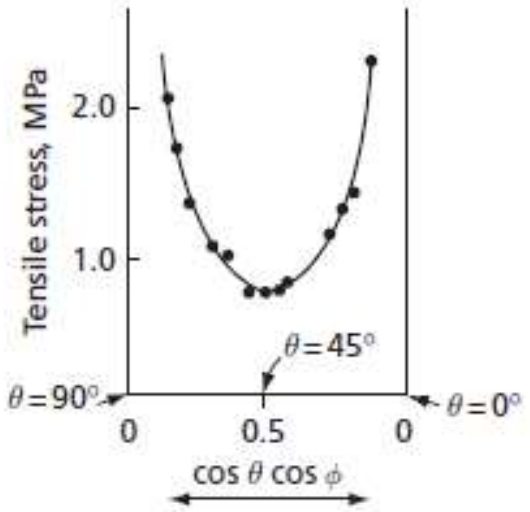

FIG. 5.15 The tensile yield point for magnesium single crystals of different orientations. Abscissae are values of the function $\cos\theta \cos\phi$. Smooth curve is for an assumed constant critical resolved shear stress of 63 psi (Burke, E. C., and Hibbard, W. R., Jr., *Trans. AIME*, **194**, 295 [1952].)

Entre direções num sistema cúbico

$$\cos\phi = \frac{h_1 \cdot h_2 + k_1 \cdot k_2 + l_1 \cdot l_2}{\sqrt{h_1^2 + k_1^2 + l_1^2} \cdot \sqrt{h_2^2 + k_2^2 + l_2^2}}$$

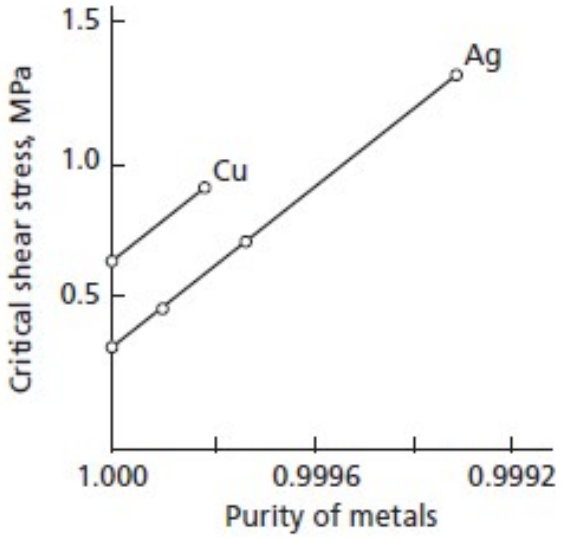

FIG. 5.16 Variation of the critical resolved shear stress with purity of the metal (After Rosi, F. D., *Trans. AIME*, **200**, 1009 [1954].)

Densidade de linhas de discordância

Explicar na lousa

Sistemas de escorregamento no CFC

4 planos {111} e 3 direções <110> = 12

TABLE 5.1 Critical Resolved Shear Stresses for Face-Centered Cubic Metals.

Metal	Purity	Slip System	Critical Resolved Shear Stress MPa
Cu*	99.999	{111} ⟨110⟩	0.63
Ag†	99.999	{111} ⟨110⟩	0.37
Au‡	99.99	{111} ⟨110⟩	0.91
Al§	99.996	{111} ⟨110⟩	1.02

*Rosi, F. D., *Trans. AIME*, 200, 1009 (1954).
†daC. Andrade, E. N., and Henderson, C., *Trans. Roy. Soc.* (London), 244, 177 (1951).
‡Sachs, G., and Weerts, J., *Zeitschrift für Physik*, **62**, 473 (1930).
§Rosi, F. D., and Mathewson, C. W., *Trans. AIME*, **188**, 1159 (1950).

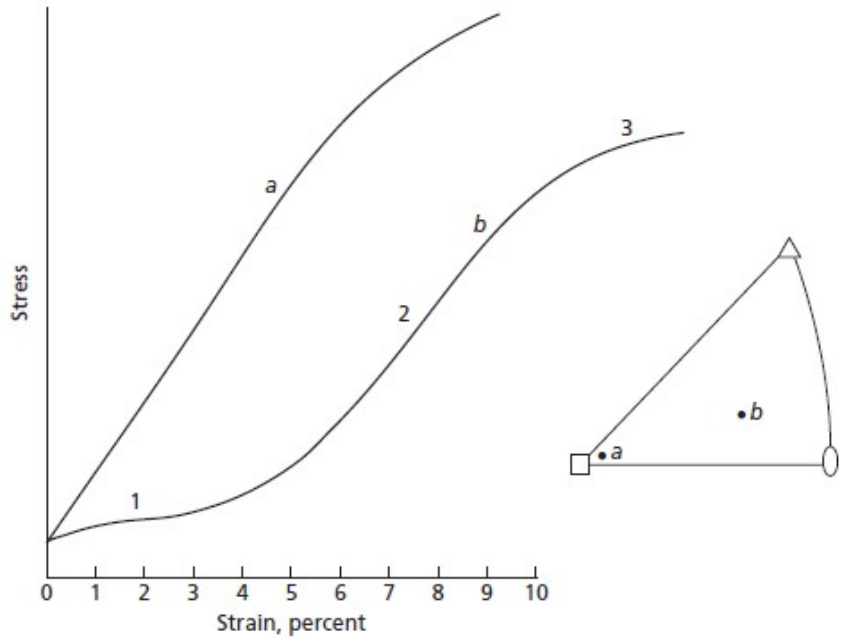

FIG. 5.17 Typical face-centered cubic single crystal stress-strain curves. Curve *a* corresponds to deformation by multiple glide from start of deformation; curve *b* corresponds to multiple glide after a period of single slip (easy glide). Crystal orientations are shown in the stereographic triangle

Sistemas de escorregamento no HCP

1 plano {0001} e 3 direções <11$\bar{2}$0> = 3

TABLE 5.2 Critical Resolved Shear Stress for Basal Slip.

Metal	Purity	Slip Plane	Slip Direction	Critical Resolved Shear Stress MPa
Zinc*	99.999	(0001)	⟨11$\bar{2}$0⟩	0.18
Cadmium†	99.996	(0001)	⟨11$\bar{2}$0⟩	0.57
Magnesium‡	99.95	(0001)	⟨11$\bar{2}$0⟩	0.43

* Jillson, D. C., *Trans. AIME*, 188, 1129 (1950).
† Boas, W., and Schmid, E., *Zeits. für Physik*, 54, 16 (1929).
‡ Burke, E. C., and Hibbard, W. R., Jr., *Trans. AIME*, 194, 295 (1952).

Sistemas de escorregamento no HCP

TABLE 5.3 The *c/a* Ratio for Hexagonal Metals.

Metal	*c/a*
Cd	1.886
Zn	1.856
Mg	1.624
Zr	1.590
Ti	1.588
Be	1.586

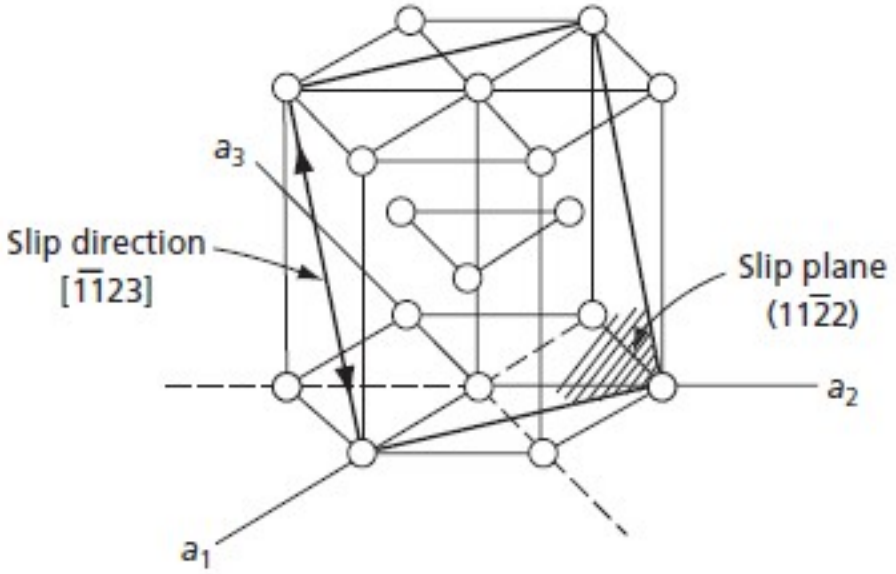

FIG. 5.18 $\{1122\}\langle 11\bar{2}3\rangle$ slip in hexagonal metals

Sistemas de escorregamento no CCC

{110} e direções <111> = 8
{112} e {123} também são ativos
Total de 48 sistemas possíveis
(são termicamente ativados)

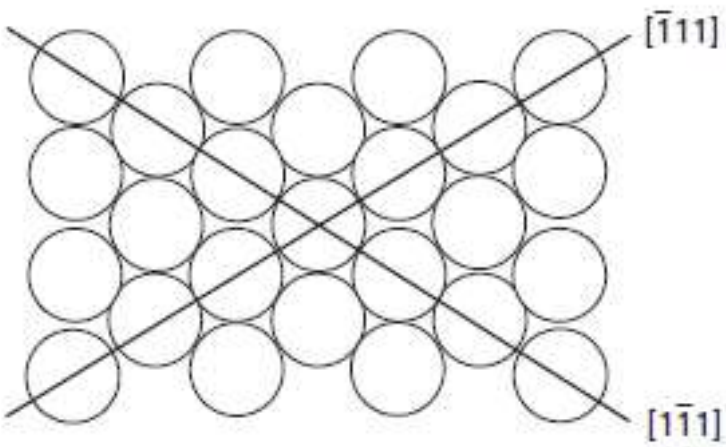

FIG. 5.19 The (110) plane of the body-centered cubic lattice

Deslizamento Cruzado

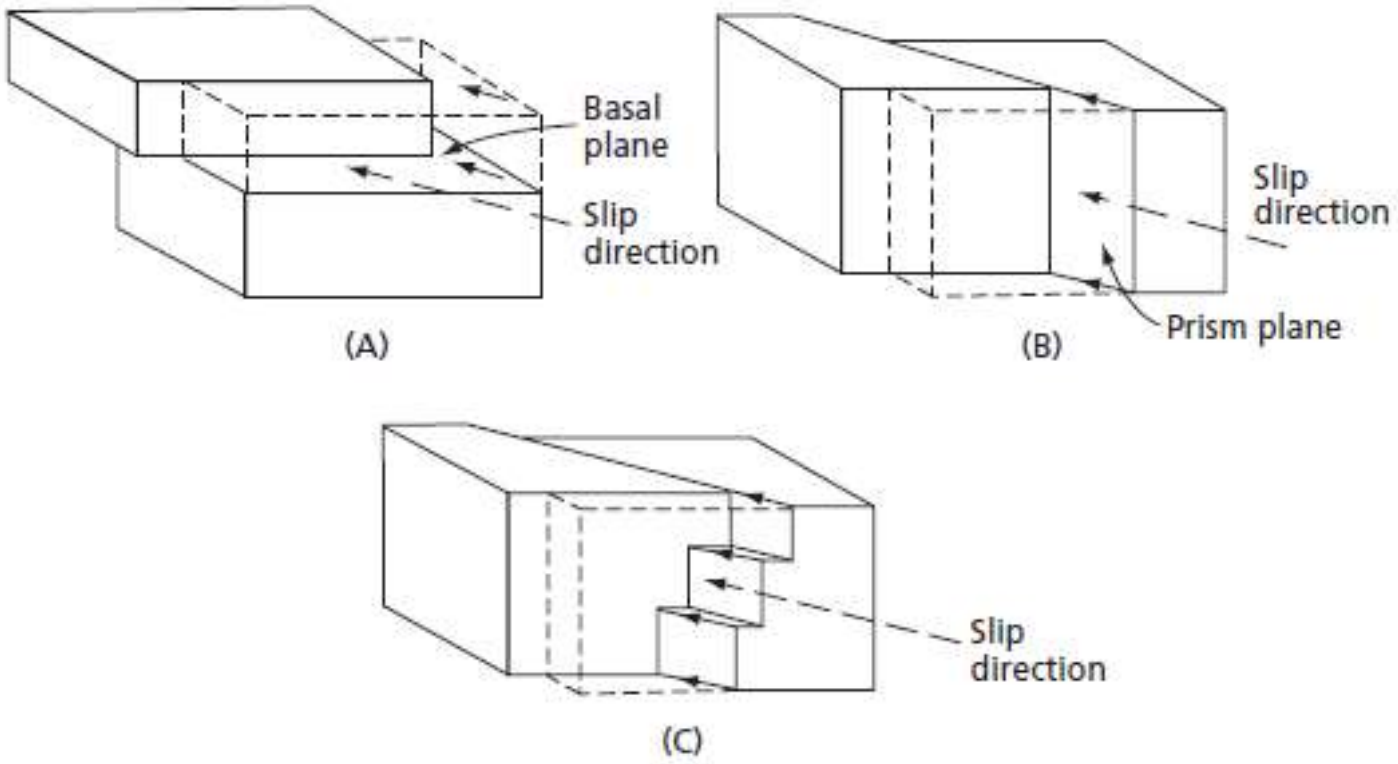

FIG. 5.20 Schematic representation of cross-slip in a hexagonal metal: **(A)** Slip on basal plane, **(B)** slip on prism plane, and **(C)** cross-slip on basal and prism planes

Deslizamento Cruzado

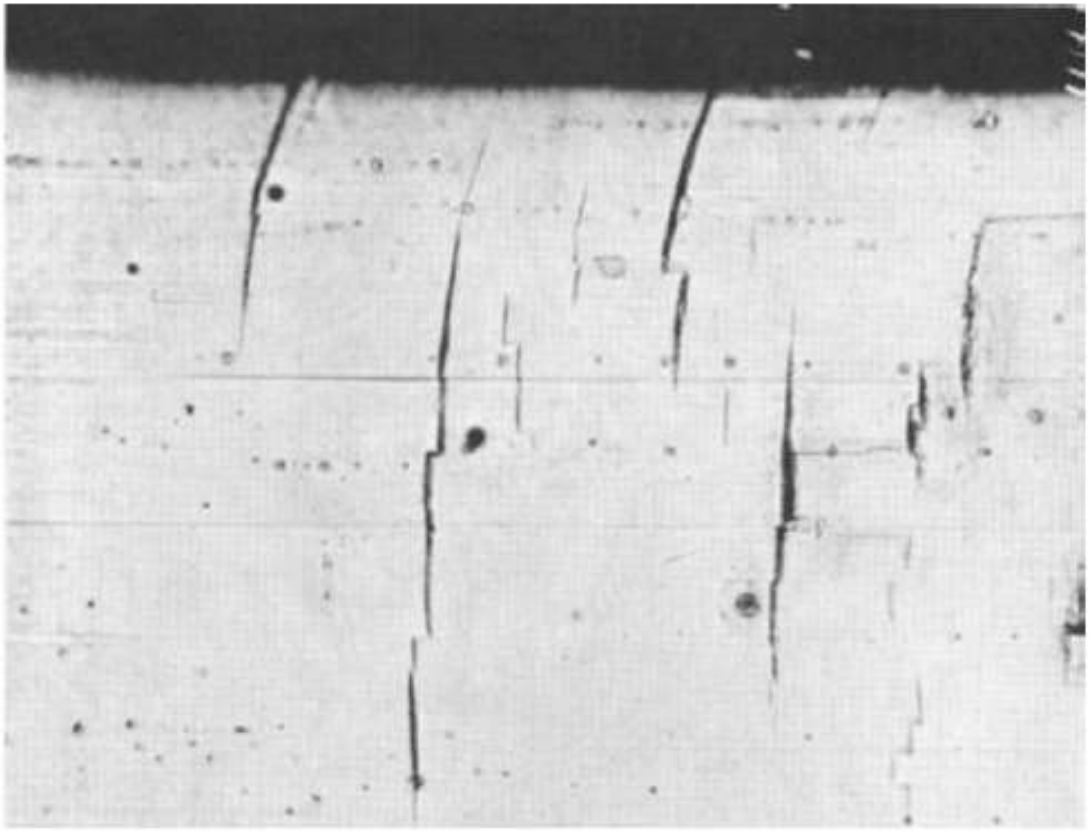

FIG. 5.21 Cross-slip in magnesium. The vertical slip plane traces correspond to the {1010} prism plane, whereas the horizontal slip plane traces correspond to the basal plane (0002). 290 × (Reed-Hill, R. E., and Robertson, W. D., *Trans. AIME*, **209** 496 [1957].)

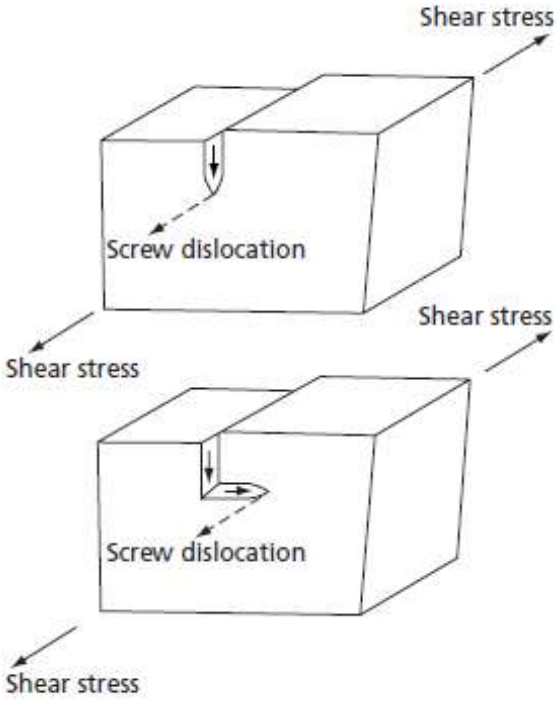

FIG. 5.22 Motion of a screw dislocation during cross-slip. In the upper figure the dislocation is moving in a vertical plane, while in the lower figure it has shifted its slip plane so that it moves horizontally

Bandas de cisalhamento

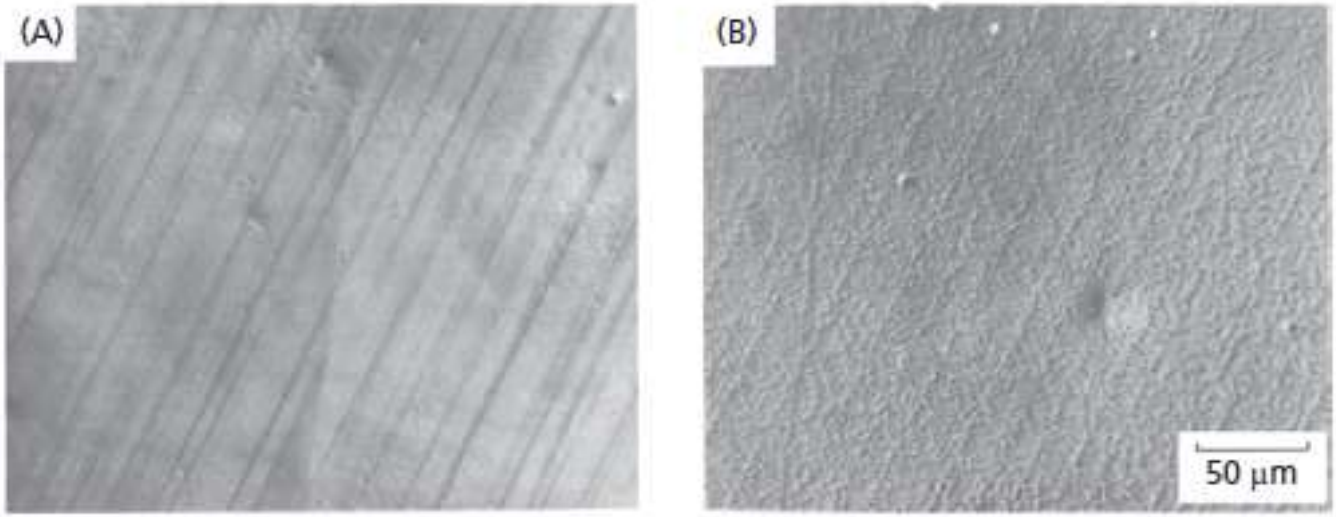

FIG. 5.23 Slip markings **(A)** and dislocation etch-pit arrays **(B)** after light deformation of gold. (From Hashimoto, S., Miura, S., and Kubo, T., *Journal of Materials Science* **11** 1501 (1976). With kind permission from Springer Science and Business Media.)

Deslizamento cruzado duplo

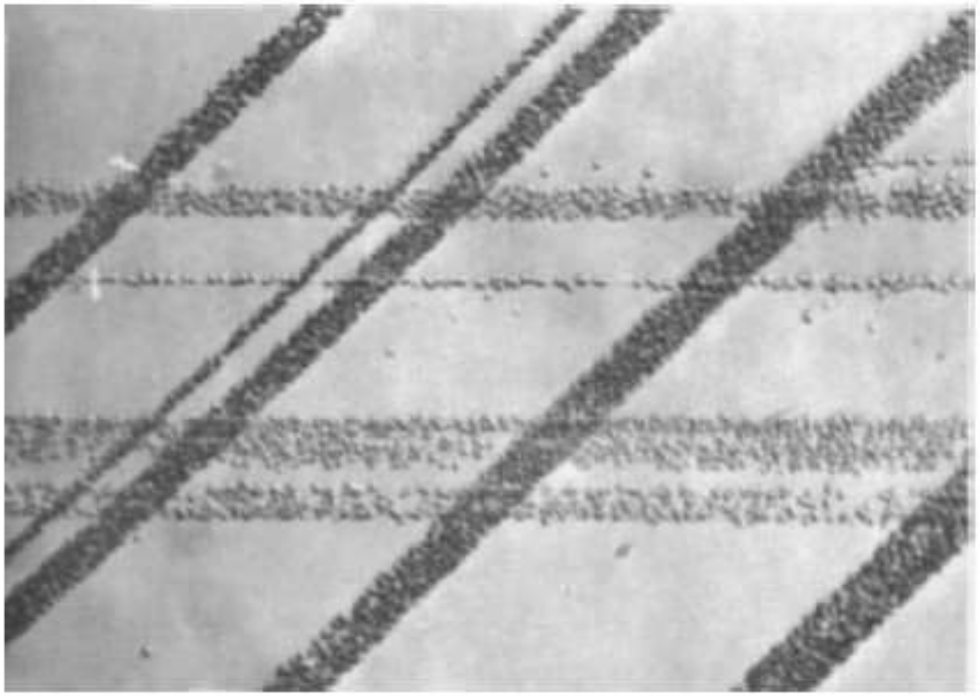

FIG. 5.24 Slip bands in LiF. Bands formed at −196 °C and 0.36 percent strain (Reprinted with permission from J.J. Gilman and W.G. Johnson, *Journal of Applied Physics*, Vol. 30, Issue 2, Page 129, Copyright 1959, American Institute of Physics)

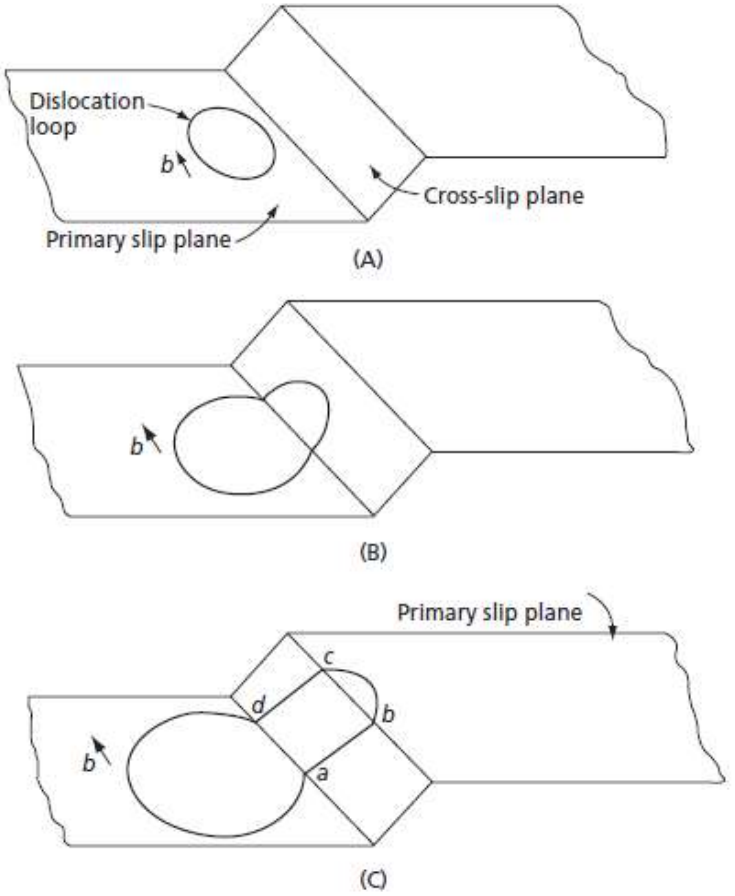

Discordâncias parciais e deslizamento cruzado

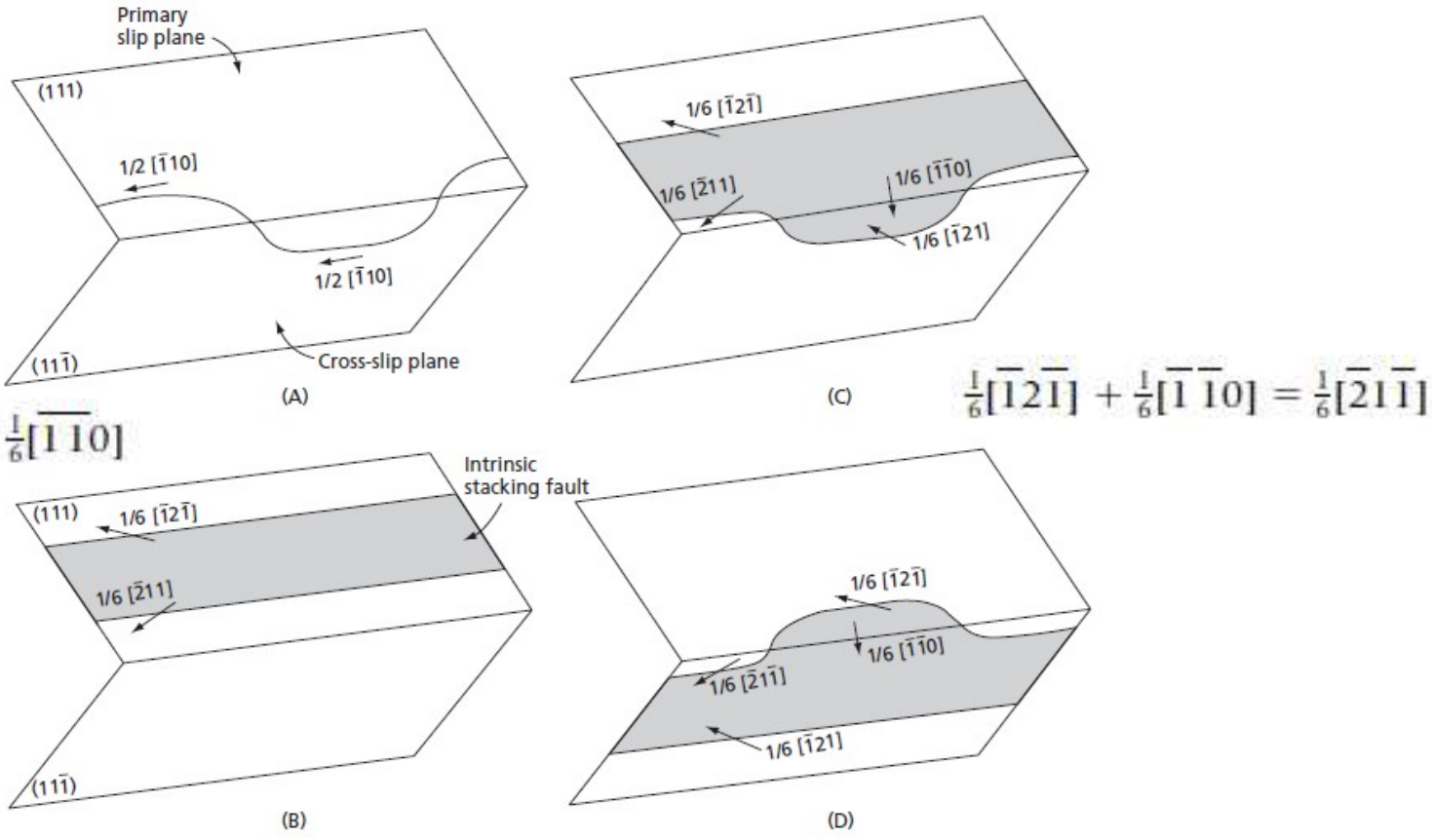

$$\tfrac{1}{6}[\bar{2}11] \rightarrow \tfrac{1}{6}[\bar{1}21] + \tfrac{1}{6}[\bar{1}\,\bar{1}0]$$

$$\tfrac{1}{6}[\bar{1}2\bar{1}] + \tfrac{1}{6}[\bar{1}\,\bar{1}0] = \tfrac{1}{6}[\bar{2}1\bar{1}]$$

FIG. 5.26 The cross-slip of an extended dislocation

Rotação do cristal durante a deformação

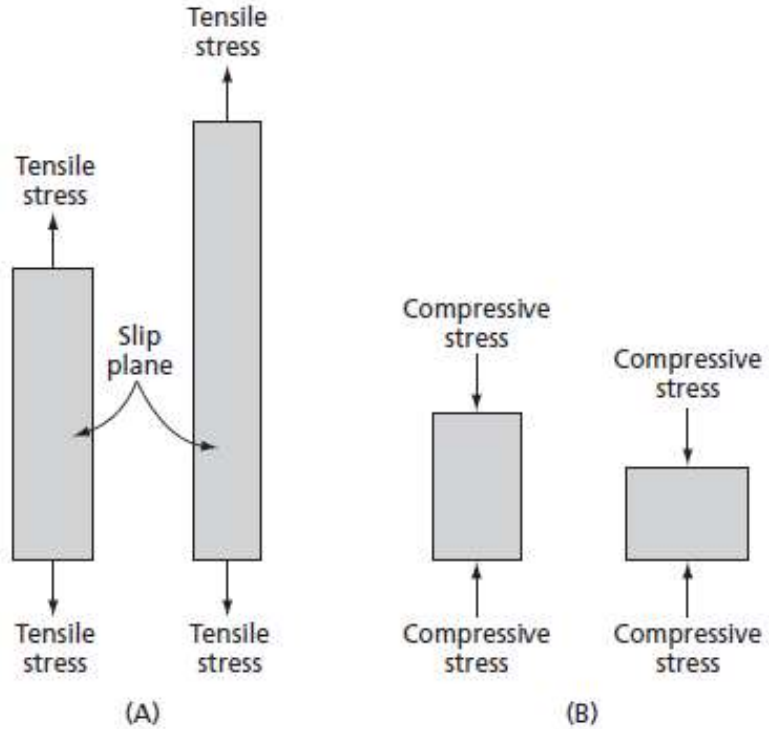

FIG. 5.27 Rotation of the crystal lattice in tension and compression

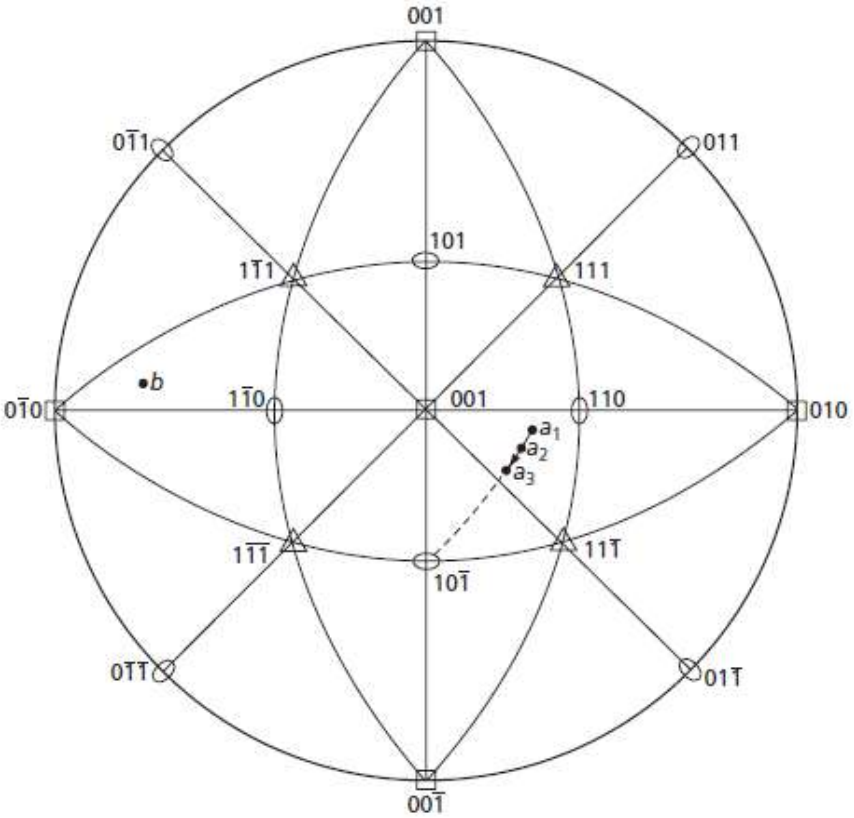

FIG. 5.28 In tension the lattice rotation is equivalent to a rotation of the stress axis (*a*) toward the slip direction. This stereographic projection shows this rotation in a face-centered cubic crystal

Rotação do cristal durante a deformação

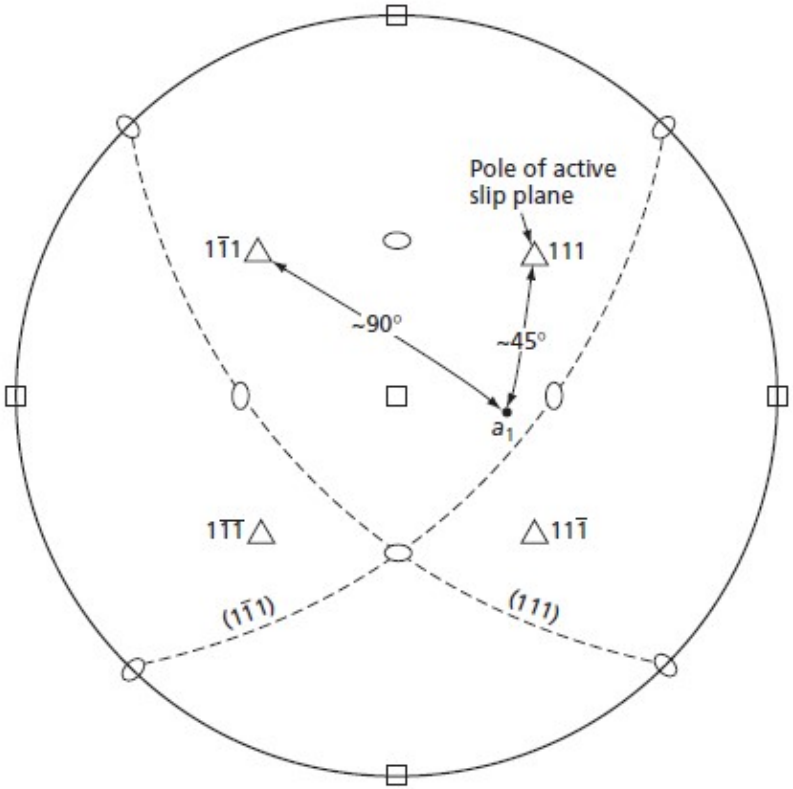

FIG. 5.29 The original stress axis orientation in Fig. 5.28 lies about 45° from the pole of the (111) plane and about 90° from the pole of (111). These are the two slip planes that contain the active slip direction

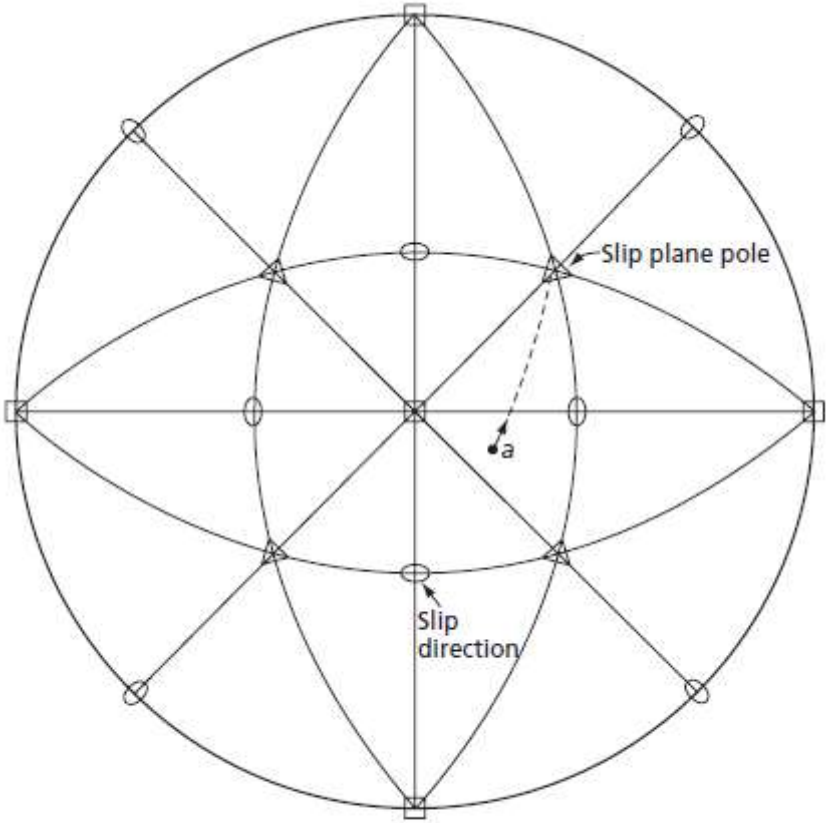

FIG. 5.30 In compression, the stress axis (*a*) rotates toward the pole of the active slip plane

Encruamento

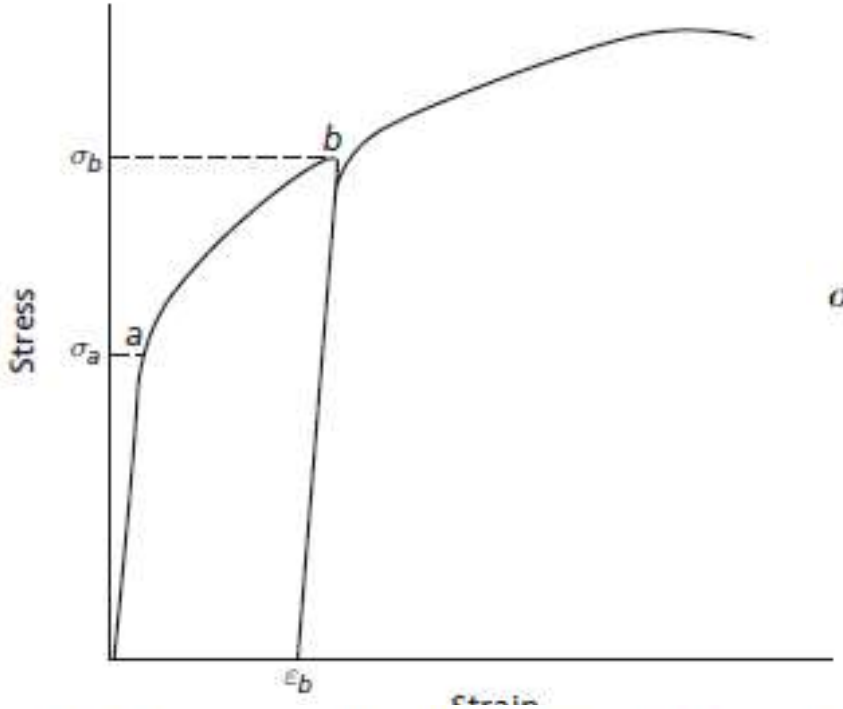

FIG. 5.32 Normally when a metal is deformed to a strain such as ϵ_b and then it is unloaded, it will not begin to deform until the stress is raised back to σ_b. The strain ϵ_b raises the flow stresses from σ_a to σ_b.

$$\sigma_t = \frac{P}{A}$$

p/ V=cte e sem estricção:

$$\sigma_t = \frac{P}{A} = \frac{Pl}{A_0 l_0} = \frac{P}{A_0}\frac{(l_0 + \Delta l)}{l_0} = \sigma(1 + \epsilon)$$

Encruamento

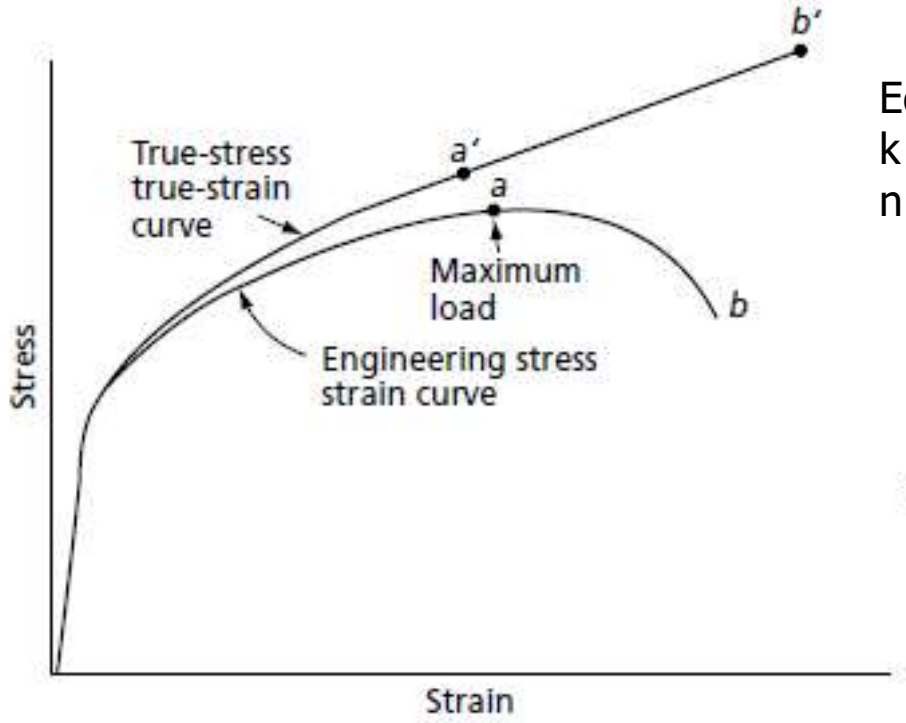

FIG. 5.33 A comparison between an engineering stress-strain curve and the corresponding true-stress and true-strain curve.

$$\sigma_t = \sigma_0 + k\varepsilon_t^{\,n}$$

Equação de Hollomon:
k – índice de resistência
n – coeficiente de encruamento

$$\epsilon_t = \int_{l_0}^{l} \frac{dl}{l} = \ln\frac{l}{l_0} = \ln(1 + \epsilon)$$

Estricção: o critério de Considère

$$dP = Ad\sigma_t + \sigma_t dA = 0$$

$$\frac{d\sigma_t}{d\epsilon_t} = \sigma_t$$

Tensão e densidade de discordâncias

$$\sigma = \sigma_0 + k\rho^{1/2}$$

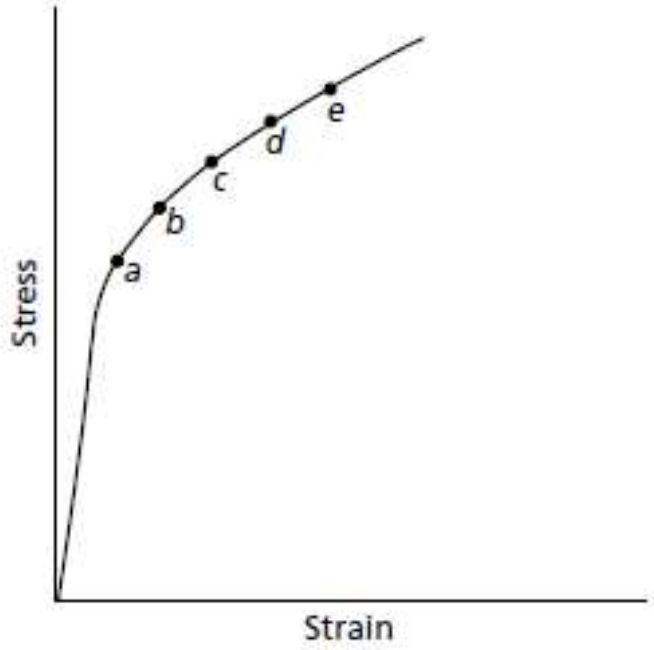

FIG. 5.34 To determine the variation of the dislocation density with strain during a tensile test, a set of tensile specimens are strained to a number of different positions along the stress-strain curve, such as points *a* to *f* in this diagram. These specimens are then sectioned to obtain transmission electron microscope foils

Tensão e densidade de discordâncias

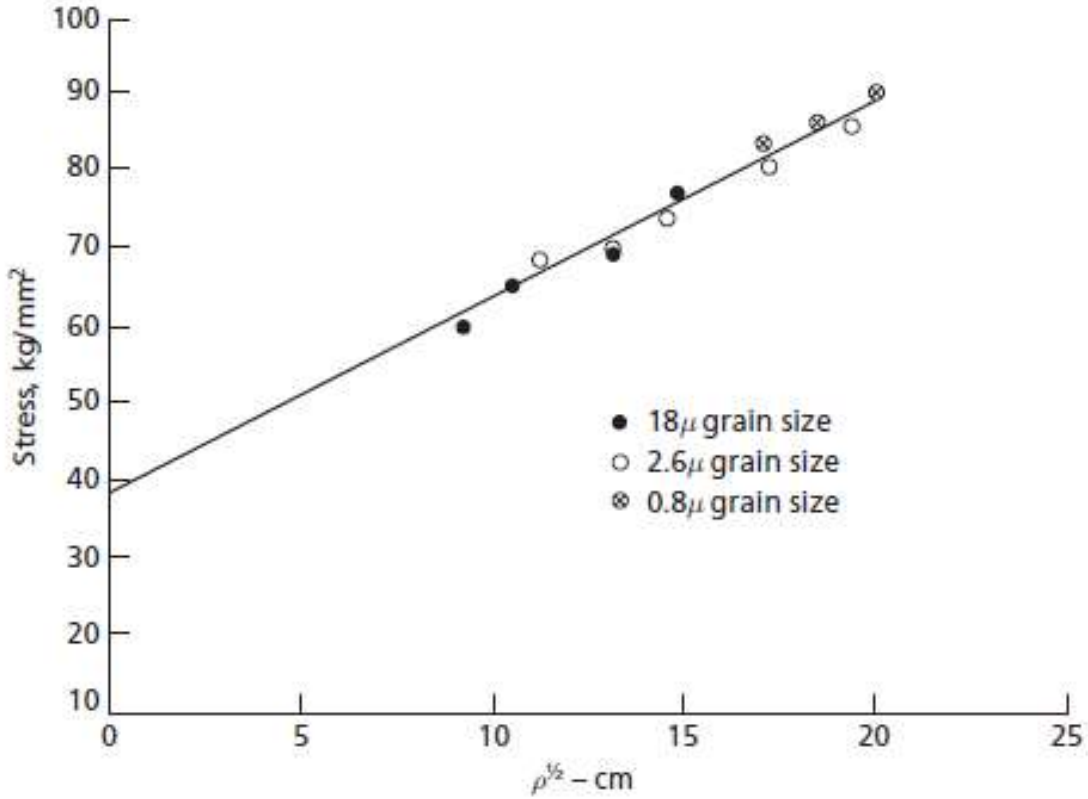

FIG. 5.35 The variation of the flow-stress σ with the square root of the dislocation density $\rho^{1/2}$ for titanium specimens deformed at room temperature, and at a strain rate of 10^{-4} sec^{-1} (After Jones, R. L., and Conrad, H., *TMS-AIME*, **245** 779 [1969].)

$$\tau = \tau_0 + k\rho^{1/2}$$

Relação de Taylor:

$$\tau \approx \frac{\mu b}{r}$$

$$\tau = \alpha \mu b \rho^{1/2}$$

$$\tau = k\rho^{1/2}$$

Equação de Orowan

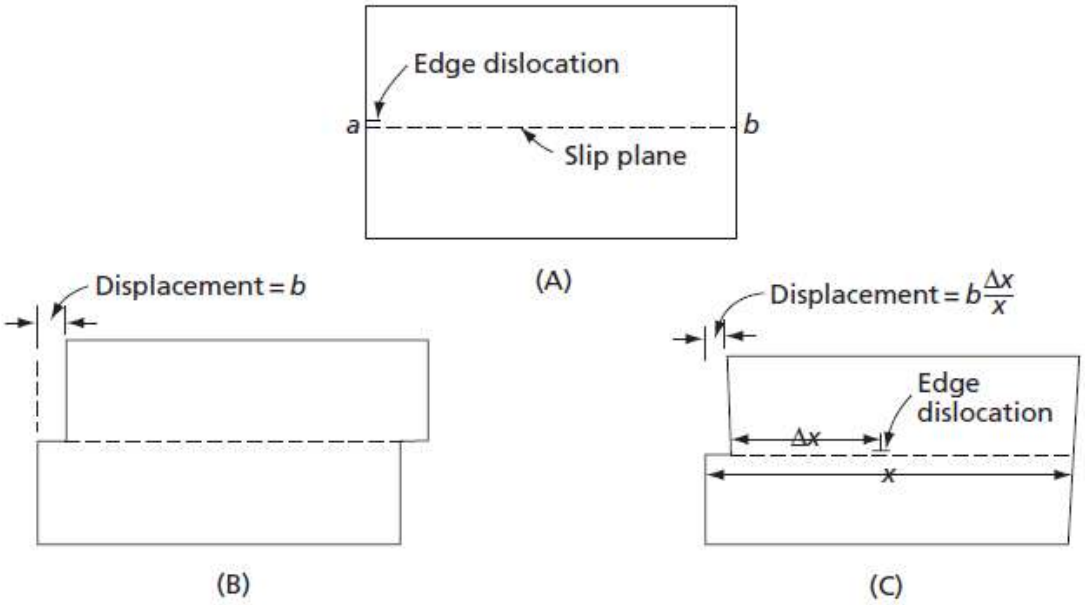

FIG. 5.36 The displacement of the two halves of a crystal is in proportion to the distance that the dislocation moves on its slip plane

$$\Delta\gamma = \frac{b\Delta A}{Az} = \frac{b\Delta A}{V}$$

$$\Delta\gamma = \frac{bnl\Delta\bar{x}}{V} = \rho b\Delta\bar{x}$$

$$\frac{\Delta\gamma}{\Delta t} = \dot{\gamma} = \rho b\bar{v}$$

$$\dot{\varepsilon} = \frac{1}{2}\dot{\gamma} = \frac{1}{2}\rho b\bar{v}$$